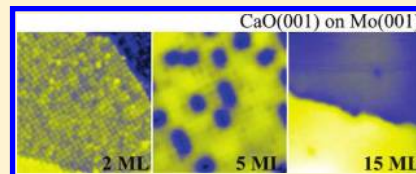


# Growth and Morphology of Calcium-Oxide Films Grown on Mo(001)

Xiang Shao, Philipp Myrach, Niklas Nilius,\* and Hans-Joachim Freund

Fritz-Haber Institut der Max-Planck Gesellschaft, Department of Chemical Physics, Faradayweg 4-6, D-14195 Berlin, Germany

**ABSTRACT:** Crystalline calcium-oxide films of various thicknesses have been grown on a Mo(001) support. The growth behavior and resulting film morphology have been characterized with low-energy electron diffraction, Auger spectroscopy, and scanning tunneling microscopy. At low film thickness, a considerable interdiffusion of Mo ions from the support into the ad-layer is revealed, giving rise to the development of a sharp  $(2 \times 2)$  superstructure with respect to the Mo(001). The Ca/Mo mixed oxide has a similar lattice parameter as the metal substrate and therefore grows pseudomorphically with a very low defect concentration. At 4–5 ML thickness, the supply of Mo from the support is interrupted and pristine CaO patches start to grow on the surface. The reemerging lattice mismatch drives the system into the Stranski-Krastanov mode, as reflected by the formation of three-dimensional oxide islands. Above 15 ML nominal thickness, the islands merge into a closed film with high surface quality and low defect concentration. The bulk character of the oxide is deduced from its band gap and optical properties, which are in good agreement with literature data reported for bulk CaO.



## 1. INTRODUCTION

CaO is a prototypical rocksalt material with various applications in heterogeneous catalysis, optoelectronics, and material sciences.<sup>1–3</sup> It is used for example to remove SO<sub>2</sub> or other sulfur-containing pollutants from the exhaust gas.<sup>4</sup> The oxide is isostructural to MgO and has comparable properties what the melting temperature, the size of the band gap or the associated optical properties concerns.<sup>5–7</sup> In contrast, both oxides largely differ in their chemical behavior, as CaO is more basic than MgO.<sup>8</sup> This difference can be traced back to the increased lattice parameter, hence the lower Madelung potential of CaO, which leads to an upshift of the valence band with respect to the vacuum energy and renders the oxide a good electron donor.<sup>9</sup> As a consequence, CaO interacts stronger with acid adsorbates, such as SO<sub>2</sub>, CO<sub>2</sub>, and H<sub>2</sub>O.<sup>10</sup> For example, while H<sub>2</sub>O forms a partly dissociated overlayer on the MgO only below 180 K, it readily dissociates on CaO even above room temperature.<sup>11</sup> CaO is also characterized by a higher state density at the surface that originates from the larger spatial expansion of the Ca 4s with respect to the Mg 3s orbital. The more delocalized electronic structure makes it easier for adsorbates to interact with the surface, which further promotes the chemical reactivity of CaO. This can be seen in the binding strength of CO<sub>2</sub>, which is negligible on MgO(001) but reaches 1 eV on the CaO surface.<sup>12</sup> Such differences in the chemical behavior despite a comparable lattice structure renders a detailed comparisons of CaO and MgO interesting from a fundamental but also an applied point of view.

Whereas a tremendous amount of work, both experimental and theoretical, has been devoted to MgO,<sup>13</sup> the number of CaO studies is surprisingly small. One reason is related to the difficulty to prepare high-quality CaO samples, such as single crystals, powders, and thin films.<sup>5,8</sup> Suitable MgO samples, however, can be easily produced in various forms. Thin films grown on metal supports play a particular role for the exploration of an oxide material; as samples can be accessed by conventional surface

science techniques without charging problems. High-quality MgO films have been prepared on various metal substrates, such as Ag(001),<sup>14</sup> Mo(001),<sup>15</sup> and Fe(001)<sup>16</sup> and formed the basis for a wealth of structural, optical, and adsorption studies on this oxide. In contrast, CaO films of similar quality are not available so far, although several attempts have been made to grow crystalline oxide layers. The most promising approaches reported in the literature are CaO films prepared by Ca deposition onto Si<sup>12,17</sup> and GaN wafers.<sup>18</sup> Furthermore, CaO has been produced by annealing TiO<sub>2</sub>(110) samples in O<sub>2</sub> in order to stimulate Ca segregation toward the surface.<sup>19</sup> In all of those studies, the structural quality of the films was controlled only with diffraction techniques, while real-space methods being much more sensitive to surface properties were not applied.

In this work, we present a new recipe to produce well-ordered CaO films on a Mo(001) support. The films were characterized with low-energy-electron diffraction (LEED), Auger spectroscopy (AES) and scanning tunneling microscopy (STM). The acquired data allowed us to develop structural models for CaO films in different growth stages. At optimal preparation conditions, the films are atomically flat and defect-poor and form a good starting point for adsorption, nucleation, and hydroxylation experiments on the CaO(001) surface.

## 2. EXPERIMENTAL SECTION

All experiments were carried out in a vacuum chamber at  $2 \times 10^{-10}$  mbar base pressure, equipped with a four-grid LEED/Auger (AES) unit, and a custom-built STM operated at liquid nitrogen temperature. The Mo(001) sample used as support was cleaned by Ar<sup>+</sup> sputtering, annealing to 1300 K in O<sub>2</sub> and flashing to 2300 K. The oxide film was prepared by Ca

**Received:** February 17, 2011

**Revised:** March 30, 2011

**Published:** April 12, 2011

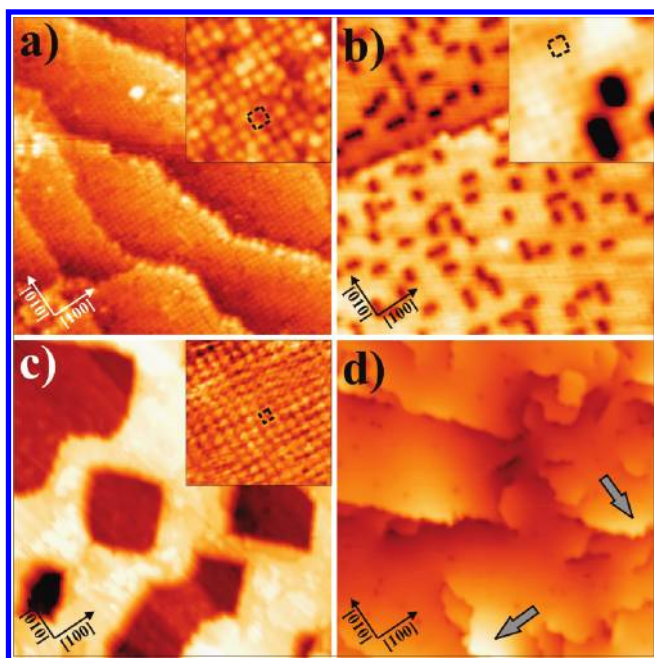


**Figure 1.** STM topographic images of CaO films with increasing thickness (a): 3 ML ( $-1.2$  V,  $25 \times 25$  nm<sup>2</sup>), (b) 5 ML (2.2 V,  $30 \times 30$  nm<sup>2</sup>), (c) 10 ML (4.5 V,  $100 \times 100$  nm<sup>2</sup>), and (d) 16 ML (4.5 V,  $100 \times 100$  nm<sup>2</sup>). The insets show atomically resolved data of selected surface regions ( $5 \times 5$  nm<sup>2</sup>) with the  $(2 \times 2)$  and  $(1 \times 1)$  unit cells being marked with dashed squares in (a,b) and (c), respectively. The arrows in (d) denote the direction of surface tilt on the faceted CaO films.

evaporation from a molybdenum crucible in  $5 \times 10^{-7}$  mbar O<sub>2</sub> onto the Mo crystal held at room temperature. The sample was then annealed to 1000 K for 10 min and quickly transferred into the cryogenic STM in order to avoid H<sub>2</sub>O and CO<sub>2</sub> adsorption from the rest gas. The oxide thickness was varied between 1 and 25 monolayer (ML), as calibrated with AES and STM measurements. The optical properties of the sample were investigated by injecting electrons from the STM tip and detecting the outgoing radiation with a grating spectrograph attached to a charge-coupled device.

### 3. RESULTS

**3.1. Thickness-Dependent Film Morphology.** The evolution of the structure and morphology of well-annealed CaO films is monitored with STM, LEED, and AES, as shown in Figures 1, 2, and 4. Four growth regimes can be distinguished as a function of the nominal layer thickness. Below 3–4 ML, the film perfectly wets the Mo(001) substrate and exhibits wide, flat terraces, being only delimited by step edges in the Mo substrate (Figure 1a). Atomically resolved STM images reveal a square pattern of  $6.3 \times 6.3$  Å<sup>2</sup> size, which corresponds to a  $(2 \times 2)$  superstructure with respect to the Mo(001). The apparent height of the atom-sized protrusions amounts to  $\sim 0.8$  Å. The same  $(2 \times 2)$  periodicity is observed in LEED (Figure 2a). The brightness and sharpness of the LEED reflexes indicate a very high surface quality, in agreement with the STM data.

The second growth stage is reached at a nominal thickness of 5 ML, but extends only for a single layer (Figure 1b). In the STM, the  $(2 \times 2)$  pattern is discernible again; however the apparent corrugation has decreased to  $\sim 0.15$  Å. In addition, the complete

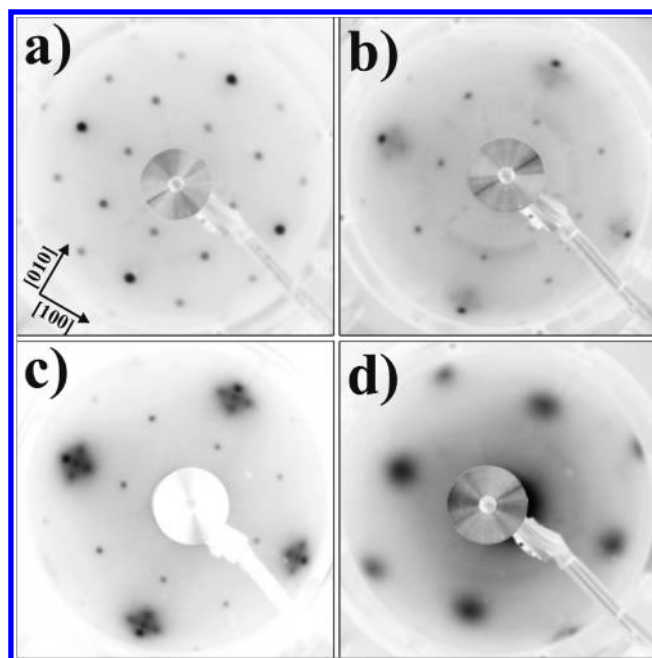


**Figure 2.** LEED pattern of a (a) 2-ML, (b) 5-ML, (c) 10-ML, and (d) 20-ML thick CaO film grown on Mo(001). The kinetic energy of the LEED electrons was set to 70 eV.

surface is covered with a regular hole-pattern. The depressions are  $\sim 2.5$  Å deep and elongated along a Mo $\langle 100 \rangle$  direction. While the width of the holes is limited to a single  $(2 \times 2)$  unit ( $6.3$  Å), their length varies between one and four  $(2 \times 2)$  cells. The holes are homogeneously arranged in the surface and have a mean center-to-center distance of  $\sim 35$  Å, corresponding to a density of  $\sim 8 \times 10^{12}$  cm<sup>-2</sup>. Surprisingly, this value is independent of the amount of deposited material, indicating that the holes are an integral part of the layer and not related to a particular Ca coverage.

Further Ca/O exposure followed by an annealing to 1000 K results in the formation of ad-islands on top of the wetting layer and marks the transition to the third growth stage (Figure 1c). The islands develop distinct square and rectangular shapes with edges running along the Mo $\langle 110 \rangle$  directions. Their initial density is as small as  $5 \times 10^{-10}$  cm<sup>-2</sup>, suggesting a very high mobility of the Ca and O species on the wetting layer. The islands exhibit a strong tendency for vertical growth and are terminated by atomically flat top facets. Whereas the weakly corrugated  $(2 \times 2)$  pattern remains detectable in between the islands, atomically resolved STM images of their top facet display a square pattern of  $3.4 \times 3.4$  Å<sup>2</sup> size and 0.1 Å corrugation. The new periodicity becomes visible also in the LEED of 5–15-ML thick films (Figure 2c), which shows a new  $(1 \times 1)$  pattern in addition to the attenuated  $(2 \times 2)$  spots of the interface layer. The  $(1 \times 1)$  reflexes are characterized by a fine-structure, composed of four Mo $[100]$ -oriented satellites. From the fact that the distance between the central spot and the satellites is independent of the kinetic energy of the LEED electrons, we deduce a certain mosaicity of the film.<sup>15</sup> Each facet hereby produces its own pattern, being displaced from the central spots by a defined tilt angle with respect to the global surface. This angle is determined to be  $3^\circ$  for a 10-ML film, but gradually decreases to zero for thicker ones. The faceting mainly occurs along the Mo $\langle 100 \rangle$  direction and can also be observed in real-space STM images (see

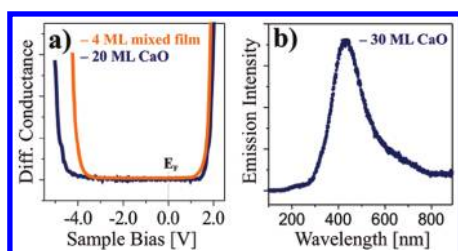


**Figure 3.** (a) Differential conductance spectra taken on 4 ML (bright curve) and 20 ML thick CaO films (dark curve). The band onsets are clearly visible. (b) Photon emission spectra acquired by injecting 150 eV electrons into a 30 ML thick CaO film (accumulation time 60 s). The emission is assigned to electron–hole pairs, radiatively decaying at low coordinated lattice sites.

arrows in Figure 1d). A more careful LEED analysis reveals that the center of the  $(1 \times 1)$  reflexes does not coincide with the original  $(1,0)$  spots of the Mo(001), but has moved inward by  $\sim 8\%$ . Translated to real space, this yields a primitive oxide cell of  $3.4 \text{ \AA}$  size, in good agreement with the STM data.

Coalescence of the CaO ad-islands starts at 8–10 ML nominal film thickness and sets the fourth growth stage. Due to the preferred island orientation, the patches merge into a characteristic stripe pattern first, being disrupted by deep rectangular holes (Figure 1c). The height difference between the island tops and the exposed wetting layer might be as large as  $15 \text{ \AA}$  for a nominally 8 ML thick film. No atomic resolution is obtained on the islands at this stage, as the tip needs to be stabilized at relatively high bias (above 4.5 V) due to the insulating nature of CaO. Increasing the Ca/O exposure leads to a gradual closing of the film and results in a flat and defect-poor CaO surface above 15 ML thickness. Closed (001) films are characterized by a plain  $(1 \times 1)$  LEED pattern that corresponds to a real-space unit cell of  $3.4 \times 3.4 \text{ \AA}^2$  (Figure 2d). The surface is permeated by a network of dislocation lines and grain boundaries, being the remnants of the island structure observed at lower thickness. Besides those line defects, only a small number of atomic-sized depressions are observed, the number of which does not exceed  $1 \times 10^{11} \text{ cm}^{-2}$ . The overall root-mean-square roughness of the film is as low as  $1 \text{ \AA}$  (Figure 1d).

**3.2. Properties of Thick CaO Films.** As the preparation of bulk-like CaO films was a main incentive of our study, we have not only probed the structural but also the electronic and optical properties of thick oxide layers. The latter are known to be particularly sensitive to a reduction of the oxide dimensionality and can therefore be taken to judge the bulk-character of the film. STM conductance spectroscopy performed with lock-in technique is used to monitor the evolution of the CaO band gap with thickness (Figure 3a). Already monolayer films exhibit a well-defined region of zero-conductance around the Fermi level, marking the emerging gap in the oxide electronic states. For 4 ML thick films, the onsets of valence and conduction bands are determined with  $-3.5$  and  $+1.75$  V, respectively, yielding a gap size of 5.25 V. This value increases to 6.5 V for a 20-ML film, which already compares well with the bulk value of 7.1 V.<sup>20</sup> The CaO/Mo(001) films exhibit the characteristic of an *n*-doped material, as the conduction band is much closer to the Fermi level than the valence band. We assign this effect to an interfacial charge transfer from the oxide film into the Mo support, which creates a positive interface dipole and induces a downward shift of the vacuum level and hence the oxide bands. The band shift

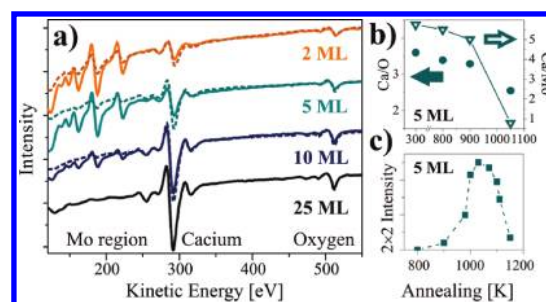


**Figure 4.** (a) Auger spectra of CaO films of various thicknesses. Dashed and solid spectra have been measured after deposition and after annealing to 1000 K, respectively. (b) Evolution of the Ca/O and Ca/Mo Auger intensities during annealing. (c) Intensity course of the  $(1/2, 1/2)$  fractional LEED spots taken as a function of the annealing temperature. The  $(2 \times 2)$  phase is fully developed at 1000 K and disappears above 1100 K due to film evaporation.

might be enhanced by Mo impurities that act as dopants in the film, the presence of which will be discussed later in this paper.

Optical properties of CaO films have been probed by detecting the photon emission induced by electron injection from the STM tip (Figure 3b). The injection of 150 eV electrons into a 30 ML thick film leads to an intense emission line at 420 nm wavelength (2.95 eV photon energy). This response agrees well with the photoluminescence measured on CaO powder samples, where it was assigned to the radiative decay of electron–hole pairs trapped at low-coordinated CaO surface sites.<sup>5</sup> The matching emission behavior detected here reflects the realization of a comparable environment for excitonic modes in our thin films. Both electronic and optical data therefore suggest that relevant properties of 20–30 ML thick films have essentially converged to the bulk characteristic of CaO.

**3.3. Chemical Composition of the CaO Films.** Finally, we have performed Auger spectroscopy as a function of film thickness and annealing temperature to determine the chemical composition of the oxide film in the different growth stages. For the sake of clarity, we start our discussion with a 25 ML CaO film that exhibits only the Ca Auger transitions at 250 (satellite) and 290 eV and the O line at 510 eV (Figure 4a, bottom curve). The Ca/O peak ratio amounts to 3.9 and remains constant over the entire annealing window of 300–1000 K. As the rocksalt monoxide is the only stable bulk phase of CaO, we assign this ratio to a one-to-one stoichiometry of Ca and O in the film. When reducing the film thickness to 10 ML, the typical Ca and O transitions prevail; however new peaks at 160, 190, and 220 eV indicate the detection of Mo Auger electrons as well (second lowest curve). The Ca/O peak ratio slightly decreases to 3.7; nonetheless the film remains more or less stoichiometric. This situation changes in the first growth stages, where the nominal film thickness drops below 5 ML. Well annealed films now exhibit a Ca/O ratio of only 2.6, implying that they are Ca-poor with respect to the bulk phase. This value even decreases to 2.2 for a bilayer film. Simultaneously, the Mo Auger transitions become more prominent (top curves).

While the Auger spectra of thick CaO films are insensitive to the annealing procedure, a distinct temperature-dependence is observed for thin films. To illustrate this evolution, we have plotted Auger spectra for as-deposited (dashed lines) and annealed films (solid lines) next to each other in Figure 4a.

Apparently, the Mo peak intensity almost triples upon annealing a 5-ML film to 1000 K, while the Ca signal reduces by  $\sim 30\%$ . However, the O signal remains nearly constant, which excludes simple film-evaporation from the surface. Taking the thick-film spectra as a reference for stoichiometric CaO, the Ca/O ratio reduces to three-to-four for thinner films after annealing. It should be noted that the as-deposited films still maintain a one-to-one stoichiometry.

Large morphological changes of the annealed films can be discarded as explanation for the altered Auger response. Both the as-prepared and tempered films homogeneously cover the surface in respective STM images and hardly exhibit any holes even at mono- and bilayer coverage. A substantial Mo oxidation as a result of a dewetting process can thus be excluded. A more plausible explanation would be the interdiffusion of Mo from the substrate into the film, where it partly replaces the Ca ions. This scenario would account for the increase in the Mo intensity and the attenuated Ca signal, as any released Ca immediately desorbs from the surface at 1000 K. An intermixing at the Mo/CaO interface during annealing is also suggested from the structural data, in particular from the LEED measurements. Mildly annealed samples display just the faint  $(1 \times 1)$  pattern of the Mo(001), indicating poor crystallinity of the oxide film, while the characteristic  $(2 \times 2)$  pattern only emerges after high temperature treatment. The same holds for the STM data, which show the  $(2 \times 2)$  superstructure only on well-annealed films. The evolution of the oxide structure with temperature can be monitored via the intensity course of the fractional  $(1/2, 1/2)$  superstructure spots, as shown in Figure 4c. They appear at around 900 K, reach maximum brightness at 1000 K and start disappearing again at even higher temperature. The attenuation of the fractional LEED spots above 1100 K comes along with a reduction of the Ca/O Auger intensities and reflects the gradual decomposition and evaporation of the film.

#### 4. DISCUSSION

On the basis of the presented experimental results and recent DFT calculations on the same system,<sup>21</sup> we suggest the following growth picture for CaO on the Mo(001) substrate. In all thickness regimes, the as-deposited or mildly annealed films are stoichiometric but amorphous, as deduced from the LEED and AES data. Crystalline films develop exclusively after thermal treatment; however, the ordering effect is accompanied by a structural and chemical modification, especially in the thin films. A driving force for the restructuring might be the lattice mismatch between ad-layer and metal support. Bulk CaO has a rocksalt structure with 4.8 Å lattice parameter ( $d_{\text{O-O}} = 3.4$  Å), which is 8% larger than the Mo(001) unit cell ( $d_{\text{Mo-Mo}} = 3.15$  Å). This mismatch inhibits a pseudomorphic growth of bulk CaO and makes substantial lattice relaxations necessary. Typical relaxation mechanisms in oxide thin films are the insertion of interfacial dislocations, as observed for MgO,<sup>15,16</sup> NiO,<sup>22</sup> or CoO films<sup>23</sup> grown on various substrates, or the development of metal-oxide coincidence structures, as in FeO/Pt(111),<sup>24</sup> alumina/Ni<sub>3</sub>Al(111),<sup>25</sup> and CeO<sub>2</sub>/Ru(0001).<sup>26</sup> Both routes are incompatible with the experimental data for CaO/Mo films that exhibits a surface without line defects but perfect interfacial registry, as reflected in the  $(2 \times 2)$  superstructure. Apparently, the growth hindrance exerted by the lattice mismatch is overcome by another means, which is suggested to be the formation of a Ca/Mo mixed oxide at the interface.

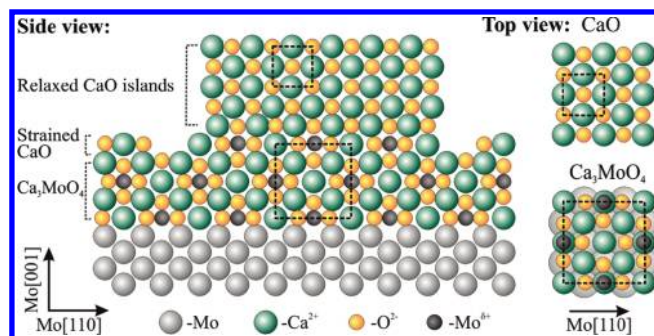


**Figure 5.** Structure model of a CaO film grown on Mo(001) displaying the first three growth stages.

**4.1. First Growth Stage.** According to the Auger spectra, well-annealed films of 2–5 ML thickness are characterized by a reduced Ca/O ratio of three-to-four but unusually strong Mo transitions. Both findings indicate a partial replacement of Ca ions by Mo, resulting in the formation of a mixed oxide phase. Yet, the experimental observations cannot be reconciled with common Ca/Mo/O bulk compounds, such as CaMoO<sub>3</sub> (perovskite) and CaMoO<sub>4</sub> (powellite), both deviating in lattice parameter and chemical composition from the present oxide system.<sup>27</sup> We therefore propose a modified CaO rocksalt structure, in which 25% of the Ca ions are replaced by Mo from the support yielding a Ca<sub>3</sub>MoO<sub>4</sub> stoichiometry (Figure 5). The incorporated Mo ions try to avoid next and second-next neighbor sites, which explains the  $(2 \times 2)$  superstructure observed in the experiment. Furthermore, the new phase can reduce the lattice mismatch with the support, as a Mo–O bond length is typically 20% shorter than a Ca–O bond (e.g., 1.9 versus 2.4 Å in CaMoO<sub>3</sub>). The eight O<sup>2-</sup> ligands around each Mo<sup>δ+</sup> center are therefore able to relax inward, providing more space for the neighboring Ca–O units (Figure 5). Such a mechanism has been confirmed with DFT that finds a lattice contraction of 5% when going from a freestanding Ca<sub>3</sub>MoO<sub>4</sub> to a CaO film.<sup>21</sup>

The better lattice match between the mixed phase and Mo(001) is however only one incentive for the Mo incorporation. A second one is the higher oxygen content of the mixed oxide with respect to a phase-separated system due to the oxidation of extra Mo atoms from the support. Both contributions will lower the formation energy of a mixed layer and promote the phase transition. It should be noted that the total energy of the system can be reduced further if surface Mo binds oxygen from the gas phase and forms molybdenyl (Mo=O) species. The presence of Mo=O groups is in fact suggested by the STM data, as their protruding nature would explain the large surface corrugation of 0.8 Å measured for films in the first growth stage. In this regard, also the point defects that are occasionally observed in STM images of the  $(2 \times 2)$  structure can be assigned, namely to O defects in the surface molybdenyl lattice (Figure 1a). We note that a similar corrugation and defect structure has been observed on the (001) surface of WO<sub>3</sub> before, where a dense array of O ad-atoms forms to compensate the intrinsic polarity of that system.<sup>28</sup>

Although the formation of a mixed oxide layer at the CaO/Mo interface seems in agreement with all experimental results presented here, a final proof for this growth behavior cannot be given without a deep chemical analysis performed with photoelectron spectroscopy.

**4.2. Second Growth Stage.** Although Mo interdiffusion into thin CaO films seems to be appropriate to compensate the lattice mismatch with the Mo(001), it is only a temporary solution and will not solve the strain problem in thicker films. One reason is the large diffusion barrier of Mo in a CaO matrix, which interrupts the Mo supply at a critical thickness. The barrier height can be approximated with 2.5 eV from the experimental transition temperature of 1000 K and a standard attempt frequency of  $1 \times 10^{13}$  Hz. Moreover, the rocksalt environment requires a cationic species in the +2 oxidation state, whereas Mo seeks for a higher charge state (up to +6 in MoO<sub>3</sub>). Not surprisingly, the formation of mixed Ca/Mo/O layers therefore stops at a critical thickness of 4–5 ML, initiating the next growth stage.

Also this stage is characterized by the development of continuous films with a faint ( $2 \times 2$ ) periodicity. The atomic corrugation has decreased to 0.15 Å, which is incompatible with a surface molybdenyl layer and suggests the absence of any Mo in the topmost plane (Figure 1b, inset). We propose that those layers are made up of pure CaO and the ( $2 \times 2$ ) pattern is only impressed by the Ca<sub>3</sub>MoO<sub>4</sub> phase underneath. Unfortunately, the model cannot be verified with Auger spectroscopy, as the technique averages over the complete film thickness and is insensitive to slight changes in the topmost layer. The growth of plain CaO without Mo impurities immediately restores the lattice mismatch in the system. This seems to be accounted for by the insertion of a high number of monolayer-deep holes into the surface layer. They are homogeneously distributed and comprise assemblies of missing Ca<sub>2</sub>O<sub>2</sub> units (Figure 1b). The introduction of such holes enables neighboring Ca–O bonds to expand toward the voids and locally reduces the lattice strain. The holes therefore fulfill a similar function as the embedded Mo ions in the first growth stage, although their density is a factor of 30 smaller.

**4.3. Third and Fourth Growth Stage.** The insertion of monolayer-deep holes is able to compensate the misfit-strain just in a single perforated CaO plane. To permanently solve the strain issue, the oxide growth crosses over into a three-dimensional mode that resembles the Stranski-Krastanov type with isolated islands growing on-top of a wetting layer.<sup>29</sup> Whereas the nuclei are still in registry with the strained surface layer of stage two, larger islands quickly adopt the lattice constant of bulk CaO, as deduced from the ( $1 \times 1$ ) periodicity in LEED and STM (Figure 1c, 2c). The interfacial relationship between the ad-islands and the wetting layer can thus be regarded as a coincidence structure with each oxide patch being anchored by a small pseudomorphic region in the center. This residual interaction is sufficient to orient the whole ad-island so that the CaO[110] direction running parallel to the [100] of the Mo support. The CaO patches in the third stage are characterized by distinct square and rectangular shapes, whereby the island edges correspond to the nonpolar CaO⟨100⟩ direction as the stable termination of rocksalt (001) surfaces.<sup>15</sup>

In the fourth and last growth stage, the isolated CaO islands merge into a flat and continuous film. Its surface is only interrupted by grain boundaries and dislocation lines arising from the coalescence of the former ad-islands. In addition, a certain number of screw dislocations become visible as step edges emanating from perfect oxide terraces. The insertion of screw cores is always accompanied by a certain faceting of the surface, which helps compensating in-plane lattice strain induced by coalescence of neighboring patches. For a 10 ML thick film, the mean tilt

angle has been determined with 3° from the LEED satellite-structure, which corresponds to an upward sloping oxide plane of 40–50 Å size that overgrows a single CaO step edge. As long as the oxide islands are of this spatial dimension, the tilt angles are discrete and produce sharp and distinct satellite spots in LEED (Figure 2c). With increasing film thickness, the distribution of tilt angles becomes wider and the satellites blur into a single broad spot (Figure 2d). The oxide film closes at around 20 ML thickness and any remnants of the interface layer disappear from the LEED and STM. At this stage, the CaO film develops true bulk behavior what lattice parameter and electronic/optical properties concerns (see Section 3.2). Still, its surface is atomically flat and defect-poor and therefore well suited for adsorption studies.

## 5. CONCLUSIONS

STM, LEED, and Auger measurements revealed a complex growth behavior of CaO on a Mo(001) support, being triggered by the relatively large lattice mismatch between both systems. In the limit of ultrathin films, mixed-oxide layers develop upon thermal treatment, whereby Mo from the substrate diffuses into the CaO rocksalt structure. Due to a reduction of the Mo–O versus Ca–O bond length, the mixed oxide has a smaller lattice parameter and grows in ( $2 \times 2$ ) registry with the Mo support. The formation of a mixed oxide stops at a critical thickness of 4–5 ML, as the Mo diffusion into the film breaks down. The reappearing lattice mismatch drives the CaO into a three-dimensional growth regime that is compatible with the Stranski-Krastanov mode. At even higher exposure, the 3D oxide islands merge into a flat and defect-poor film, characterized by structural and electronic parameters that are similar to the ones of bulk CaO.

The CaO/Mo(001) films display several fascinating properties in the various growth stages that need to be further investigated in future. At low thickness, the Mo impurities inside the CaO matrix give rise to a number of unusual electronic, optical and magnetic properties that are intrinsically connected to the Mo *d* levels located in the oxide band gap.<sup>30</sup> The Mo dopants will also alter the adsorption and hence the chemical characteristic of ultrathin oxide films. At higher film thickness, bulk-like CaO surfaces with extremely high quality can be prepared, being suited for adsorption and growth experiments with metal atoms and molecules. Studies on well-characterized CaO(001) surfaces have not been reported in the literature so far, in sharp contrast to the extensively examined MgO(001). A comparison of both systems might provide new insights into the relationship between lattice parameter, electronic properties and chemical reactivity of iso-structural oxide materials.

## AUTHOR INFORMATION

### Corresponding Author

\*E-mail: nilius@fhi-berlin.mpg.de.

## ACKNOWLEDGMENT

We are grateful to G. Pacchioni for various instructive discussions and acknowledge financial support from the Excellence initiative “UNICAT” of the DFG.

## REFERENCES

- (1) Medeiros, S. K.; Albuquerque, E. L.; Maia, F. F., Jr.; Caetano, E. W. S.; Farias, G. A.; Freire, V. N.; Cavada, B. S.; Pessati, M. L.; Pessati, T. L. P. *Microelectron. J.* **2005**, *36*, 1058.
- (2) Martín Alonso, D.; Mariscal, R.; López Granados, M.; Maireles-Torres, P. *Catal. Today* **2009**, *143*, 167.
- (3) Kawashima, A.; Matsubara, K.; Honda, K. *Bioresour. Technol.* **2009**, *100*, 696.
- (4) Lee, Y. C.; Montano, P. A.; Cook, J. M. *Surf. Sci.* **1984**, *143*, 423.
- (5) Bolorizadeh, M. A.; Sashin, V. A.; Kheifets, A. S.; Ford, M. J. *J. Electron. Spectrosc. Relat. Phenom.* **2004**, *141*, 27. Albuquerque, E. L.; Vasconcelos, M. S. *J. Phys.: Conf. Ser.* **2008**, *100*, 042006.
- (6) Stankic, S.; Bernardi, J.; Diwald, O.; Knözinger, E. *J. Phys. Chem. B* **2006**, *110*, 13866.
- (7) Trevisanutto, P. E.; Sushko, P. V.; Beck, K. M.; Joly, A. G.; Hess, W. P.; Shluger, A. L. *J. Phys. Chem. C* **2009**, *113*, 1274.
- (8) Paganini, M. C.; Chiesa, M.; Dolci, F.; Martino, P.; Giamello, E. *J. Phys. Chem. B* **2006**, *110*, 11918.
- (9) Pacchioni, G.; Ricart, J. M.; Illas, F. *J. Am. Chem. Soc.* **1994**, *116*, 10152. Pacchioni, G.; Sousa, C.; Illas, F.; Parmigiani, F.; Bagus, P. S. *Phys. Rev. B* **1993**, *48*, 11573.
- (10) Chiesa, M.; Giamello, E.; Murphy, D. M.; Pacchioni, G.; Paganini, M. C.; Soave, R.; Sojka, Z. *J. Phys. Chem. B* **2001**, *105*, 497.
- (11) Liu, P.; Kendelewicz, T.; Brown, G. E., Jr.; Parks, G. A. *Surf. Sci.* **1998**, *412–413*, 287. Liu, P.; Kendelewicz, T.; Brown, G. E., Jr.; Parks, G. A.; Pianetta, P. *Surf. Sci.* **1998**, *416*, 326.
- (12) Ochs, D.; Braun, B.; Maus-Friedrichs, W.; Kempter, V. *Surf. Sci.* **1998**, *417*, 406.
- (13) Pacchioni, G. *Surf. Rev. Lett.* **2000**, *7*, 277.
- (14) Schintke, S.; Messerli, S.; Pivetta, M.; Patthey, F.; Libjoulle, L.; Stengel, M.; de Vita, A.; Schneider, W. D. *Phys. Rev. Lett.* **2001**, *87*, 276801.
- (15) Benedetti, S.; Benia, H. M.; Nilius, N.; Valeri, S.; Freund, H. J. *Chem. Phys. Lett.* **2006**, *430*, 330.
- (16) Vassent, J. L.; Dynna, M.; Marty, A.; Gilles, B.; Patrat, G. *J. Appl. Phys.* **1996**, *80*, 5727.
- (17) Bebensee, F.; Voigts, F.; Maus-Friedrichs, W. *Surf. Sci.* **2008**, *602*, 1622.
- (18) Losego, M. D.; Mita, S.; Collazo, R.; Sitar, Z.; Maria, J. P. *J. Vac. Sci. Technol. B* **2007**, *25*, 1029.
- (19) Nörenberg, H.; Harding, J. H. *Phys. Rev. B* **1999**, *59*, 9842.
- (20) Whited, R. C.; Flaten, C. J.; Walker, W. C. *Solid State Commun.* **1973**, *13*, 1903.
- (21) Shao, X.; Myrach, P.; Nilius, N.; Freund, H. J.; Martinez, U.; Giordano, L.; Pacchioni, G. 2011, submitted for publication.
- (22) Schoiswohl, J.; Zheng, W.; Surnev, S.; Ramsey, M. G.; Granozzi, G.; Agnoli, S.; Netzer, F. P. *Surf. Sci.* **2006**, *600*, 1099.
- (23) Torelli, P.; Soares, E. A.; Renaud, G.; Valeri, S.; Guo, X. X.; Luches, P. *Surf. Sci.* **2007**, *601*, 2651.
- (24) Weiss, W.; Ranke, W. *Prog. Surf. Sci.* **2002**, *70*, 1.
- (25) Schmid, M.; Kresse, G.; Buchsbaum, A.; Napetschnig, E.; Gritschneider, S.; Reichling, M.; Varga, P. *Phys. Rev. Lett.* **2007**, *99*, 196104.
- (26) Castellarin-Cudia, C.; Surnev, S.; Schneider, G.; Podlucky, R.; Ramsey, M. G.; Netzer, F. P. *Surf. Sci.* **2004**, *554*, L120.
- (27) We have also considered an alternative model, in which a  $(2 \times 2)$  array of cationic or anionic vacancies is present in the interfacial CaO plane. Such growth motives have been observed for other highly mismatched metal-oxide systems, e.g., NiO on Pd(100). However, recent DFT calculations suggested that a defective interface is thermodynamically unstable with respect to a strained but stoichiometric layer, reflecting the nonreducible character of CaO.<sup>21</sup>
- (28) Jones, F. H.; Rawlings, K.; Foord, J. S.; Egdell, R. G.; Pethica, J. B.; Wanklyn, B. M. R.; Parker, S. C.; Oliver, P. M. *Surf. Sci.* **1996**, *359*, 107. Jones, F. H.; Dixon, R. A.; Brown, A. *Surf. Sci.* **1996**, *369*, 343.
- (29) Ritter, M.; Ranke, W.; Weiss, W. *Phys. Rev. B* **1998**, *57*, 7240.
- (30) Henderson, B.; Imbusch, G. F. *Optical Spectroscopy of Inorganic Solids*; Clarendon Press: Oxford, 1989.